

Predicting Molecular Interactions  
with Nonporous and Nanoporous Carbon  
using Computational Chemistry

by  
Katherine A. Ziegler

Departmental Honors Thesis  
The University of Tennessee at Chattanooga  
Department of Chemistry

Project Director: Tom Rybolt  
Examination Date: November 11, 2005

Committee Members:

Tom Rybolt  
Robert Mebane  
Doug Kutz  
George Helton

Examining Committee Signatures:

---

Project Director

---

Department Examiner

---

Department Examiner

---

Liaison, Departmental Honors Committee

---

Chairperson, University Departmental Honors Committee

## Contents

Abstract	2
Introduction	5
Theory	9
Experimental	13
Analysis and Results	16
Discussion	22
Conclusion	25
References	26
Tables	28
Figures	37

## Abstract

The gas-solid interaction energies,  $E^*$ , of two carbon surfaces (Carbosieve SIII and Carbopack C, both produced by Supelco, Inc.) were available from gas chromatography values. Gas chromatography is the process of flowing gas through a column packed with carbon powder or another stationary phase in order to obtain retention times. The calculated interaction energies,  $E_{cal}^*$ , of the two surfaces were determined using CAChe (Computer Aided Chemistry molecular modeling software, version 6.1.10, Fujitsu) in conjunction with two different surface models, flat and porous. The experimental interaction energy values were plotted against the corresponding calculated values for each surface model to determine if the CAChe program could adequately represent each surface. The ratio of  $E_{cal}^*/E^*$  was determined for each of the gases tested and the percent error for the deviation between calculated and experimental values determined.

Before surface testing within CAChe could occur, a testable (flat, uniform) graphite surface had to be constructed. The number of rings and layers to adequately represent the gas-surface interactions was determined. This was done by testing surface interactions with Ne, Ar, Kr, and Xe to determine the number of rings and layers at which energy values were not significantly affected by increasing the surface size. The adequate number of rings and layers were found to be 127 and three, respectively. After constructing appropriate representative structures, the calculated interaction energy values,  $E_{cal}^*$  values, were determined in CAChe and compared with experimental values of  $E^*$ . In the case of Carbosieve SIII, different model pore

sizes were tested to determine which pore size provided data more closely fitting the experimental data on Carbosieve SIII. The most appropriate pore size was found to be 5.0 Angstroms or 0.50 nm.

Carbosieve SIII was experimentally determined by Micromeritics Company, using nitrogen adsorption, to be a nanoporous carbon surface with most pores measuring around 0.55 nm and a surface area of 995 m<sup>2</sup>/g. The flat surface model gave an average percent error of 45% and r<sup>2</sup> of 0.864 for plots of the experimental interaction energy values versus the CAChe calculated values, while the porous surface model of 0.55 nm gave an average percent error equal to 38% and r<sup>2</sup> of 0.962. From these results, it was determined that the porous surface model better represents Carbosieve SIII.

Carbopack C, experimentally determined to be a flat carbon surface with an area of 10 m<sup>2</sup>/g, gave an average percent error of 30% and r<sup>2</sup> of 0.945 for the experimental interaction energy values versus the calculated values for the porous surface model. In comparison, the flat surface model gave an average percent error equal to 10% and an r<sup>2</sup> value of 0.927. From these results, it was determined that the flat surface provided data more closely fitting the experimental data on Carbopack C.

The data found shows that through comparison of several factors, r<sup>2</sup> values, slopes, Ecal\*/E\* ratios, and percent errors, CAChe software can accurately correlate physical properties of molecules. This determination has important scientific potential in that it could make it possible to take physical properties calculated

through CAChe, and use those values to predict gas chromatographic retention times without having to determine the values experimentally within the lab.

## Introduction

An important aspect of physical chemistry involves understanding and predicting the adsorption of gas molecules on carbon surfaces (1). Gas chromatography is the process of flowing helium and an injected sample gas through a column packed with carbon powder or another stationary phase, to obtain retention times. As a molecule nears a surface, it experiences an attraction from van der Waals forces (VDW). These van der Waals forces are weak but have a long range. The strength of these attractions, between the molecule and the carbon surface, directly affects the gas chromatographic retention time of the molecule. A slower moving molecule experiences a stronger attraction to the carbon surface, and thus a longer retention time, than a faster moving molecule.

Adsorbates, the gas molecules, are attracted to the surface of the adsorbent as a result of these weak interactive forces. These attractive forces cause the adsorbate to approach the adsorbent until a certain point, at which the forces between the adsorbate and adsorbent become repulsive. This idea of an optimum distance between the gas molecules and the surface is represented by the Lennard-Jones potential energy well, shown in Figure 1. As can be seen in Figure 1, as the gas molecule approaches the surface, the energy noticeably decreases and then increases. The lowest point of the potential well represents the gas-solid interaction energy,  $E^*$ , which occurs at the equilibrium separation of the gas and the solid. This equilibrium separation is somewhat analogous to the bond distance in a compound.

Each summer, Dr. Rybolt's research colleague, Dr. Howard Thomas, and his research student work with gas chromatography (GC) to produce experimental  $B_{2s}$  values, second gas-solid virial coefficient values, which are related to the strength of gas-solid interactions. Larger  $B_{2s}$  values indicate stronger gas-solid attractions. The gas-solid interaction energy values,  $E^*$ , can be calculated from  $B_{2s}$  values by plotting  $\ln B_{2s}$  versus  $1/T$ , where  $T$  is the temperature in units of Kelvin. The slope of the linear regression produced is equal to  $E^*$ . Essentially, my work is aimed at relating the structure of molecules and the nature of carbon surfaces through equations and calculations to these experimentally measured properties.

The study of relating the structure and nature of carbon surfaces with experimental properties for use in adsorption has many important applications. The question of hydrogen storage methods in reference to the operation of fuel cell driven cars could be addressed through the use of hydrogen-carbon attraction. This attraction, if strong enough, applied to carbon nanotubes could possibly allow these long, carbon tubes with rounded, closed ends to store the hydrogen until needed.

In addition to hydrogen storage, this type of research also has the possibility of providing data which could lead to the production of more effective modeling of chemical warfare protection through gas masks and suits filled with carbon powder or fibers. Environmental clean-up is another area where such research could prove to be very useful, since it is based on the interaction of organic molecules with solid surfaces. Carbon filters can be used to remove organic pollutants from water or air. In the area of nanotechnology it will also be important to understand the interactions

of small molecular machines with solid surfaces (2). This research also offers exciting advances for general methods of research by decreasing the need for experimental values. This advance offers scientists the ability to focus on possible applications of the data while reducing the time spent analyzing laboratory results.

The interactions of molecules with graphite surfaces have been investigated in recent studies (3-14). Using a molecular mechanics method with MSI Insight II program, Shuxia et al. found that copper phthalocyanine (CuPc) and  $C_{34}H_{70}$  adsorb on highly oriented pyrolytic graphite (HOPG) with adsorption energies of  $-61.40$  kcal/mol and  $-61.43$  kcal/mol, respectively (3). The physisorption of  $O_2$  molecules onto graphite and on (8, 0) single-walled carbon nanotubes has also been examined, using spin-polarized density functional calculations (4). It was found to be weak by Sorescu and Jordan, with an adsorption energy of only 0.9 kcal/mol (4). Using the Gaussian98 package, Montoya et al. examined NO adsorption on a single-layer graphene and found adsorption energies of 90.1 kcal/mol from the Hartree-Fock method and 44.1 kcal/mol using density functional theory (5). High-resolution adsorption analysis was used by Murata et al. to determine the interaction potential of  $N_2$  on both a flat graphite surface, -1150 K, and in nanopores of the single wall carbon nanohorn particles, -1690 K (6).

In my work, the experimental  $E^*$  values, determined from the linear regressions of  $\ln B_{2s}$  values versus  $1/T$ , were compared with calculated interaction energy values,  $E_{cal}^*$ , found using CAChe (Computer Aided Chemistry, version 6.1.10, Fujitsu). This was done with two surface models: Carbosieve SIII and

Carbopack C. In both cases, the surface was modeled within CAChe and tested with the molecules for which we had experimental data. A porous surface and flat surface were both tested to see whether the flat surface or nanoporous surface model provided data more closely fitting the experimental data for the Carbosieve SIII and Carbopack C.

## Theory

Gas chromatography is the process of flowing helium and an injected sample gas through a column packed with carbon powder or another stationary phase to obtain retention times. These retention times are important because they depend on the strength of the attraction between the sample and the stationary phase. The stronger the attraction, the longer the sample will stay on the column and thus the longer the retention time. Thus gas chromatography can be used for the analysis of adsorption.

In the Henry's Law region of low coverage adsorption, the retention time is given by

$$t = t_s - t_m \quad (1)$$

where  $t_m$  is the time from injection to detection for the marker gas, or neon, which has negligible gas-solid interactions and  $t_s$  is the time from injection to detection for the sample gas. Using Equation 1 for  $t$ , the retention time of an adsorbate gas can be used to calculate the  $B_{2s}$  value using the equation

$$B_{2s} = (t F_1/m) \quad (2)$$

where  $F_1$  ( $\text{cm}^3/\text{s}$ ) is the corrected flow rate of the gas chromatographic column, and  $m$  (g) is the mass of the solid adsorbent.

Since there is a minimum of interactions between the gas molecules in the Henry's Law region of low coverage, the number of moles of adsorbate,  $n_{\text{ad}}$  (moles adsorbate/ g adsorbent), that have adsorbed on the solid surface can be determined

using the second gas-solid virial coefficient or  $B_{2s}$  value. The moles adsorbed,  $n_{ad}$ , is given by

$$n_{ad} = B_{2s} (P/RT) \quad (3)$$

where  $P$  (kPa) is the pressure,  $R$  (0.0821 L atm/mol K or 8319 kPa cm<sup>3</sup>/mol K) is the ideal gas constant, and  $T$  (K) is the temperature.

For a uniform, flat surface  $B_{2s}$  can be expressed as

$$B_{2s} = Az^* \int [\exp(-u_{1s}(y)/kT) - 1] dy \quad (4)$$

where  $A$  is the area of the adsorbent,  $z^*$  is the internuclear gas-solid separation,  $u_{1s}$  is the gas-solid interaction potential,  $y$  is a reduced variable ( $y = z/z^*$ ),  $z$  is the gas-solid separation,  $k$  is the Boltzmann constant, and  $T$  is the temperature. From Equation 4, it can be seen that as  $u_{1s}$  deepens the value of  $B_{2s}$  increases, thus signifying a stronger attraction of the gas to the solid (16).

The interaction between a gas and a solid given by Equation 4 can be expressed using the Lennard-Jones potential as

$$u_{1s}(y)/k = E^* \left[ \frac{n}{(n-m)} \right] \left( \frac{n}{m} \right)^{[m/(n-m)]} \\ \times \left\{ y^{-n} \left( \frac{n}{m} \right)^{[n/(m-n)]} - y^{-m} \left( \frac{n}{m} \right)^{[m/(m-n)]} \right\} \quad (5)$$

where  $E^*$  is the gas-solid interaction energy expressed in units of Kelvin,  $m$  is the attractive term,  $n$  is the repulsive term, and  $y$  is a reduced variable ( $y = z/z^*$ ). Using these parameters, the specific depth of the Lennard-Jones potential energy well can be determined (16).

In general, Equation 4 and Equation 5 can be combined to give

$$B_{2s} = Az^* I(E^*, T) \quad (6)$$

where  $A$  is the area,  $z^*$  is the equilibrium separation,  $E^*$  is the interaction energy expressed in units of Kelvin,  $T$  is the temperature, and  $I(E^*, T)$  is an integral function of temperature and interaction energy. Experimental  $B_{2s}$  values at different temperatures can be used with Equation 6 to avoid size bias. This can be done by selecting the best value of  $E^*$  such that the value of the standard deviation of  $\log(Az^*)$  is minimized for a given adsorbate.

The flat single-surface model that has been discussed thus far is accurate for some surfaces, but use of a flat two-surface model can improve accuracy in some instances. In the flat two-surface model, the surface is assumed to contain higher and lower energy sites, this is in opposition to the assumed uniformity of the flat single-surface model. High energy sites have the potential of having a significant influence on the adsorptive capabilities of the surface and thus the amount of gas adsorbed.

In the two-surface approach, the total  $B_{2s}$  value can be separated into two contributions, the high energy and the low energy areas of the surface. This is expressed as

$$B_{2s} (\text{Total}) = B_{2s} (\text{Low Energy}) + B_{2s} (\text{High Energy}). \quad (7)$$

When combined with Equation 6, this gives

$$B_{2s} (T) = A_1 z^* I_1(E_1^*, T) + A_2 z^* I_2(E_2^*, T) \quad (8)$$

where  $I_1$  is the low energy integral,  $E_1^*$  is the interaction energy of surface one, the low energy portion of the surface,  $I_2$  is the high energy integral,  $E_2^*$  is the interaction energy of surface two, the high energy portion of the surface, and  $A$  is the total

surface area, the sum of  $A_1$ , the lower energy surface area, and  $A_2$ , the higher energy surface area.

If the percentage of the area for surface two is defined as  $x$ , then  $A_1 = (1-x)A$ ,  $A_2 = xA$ , and

$$Az^* = B_{2s}(T)/[(1-x)I_1(E_1^*, T) + xI_2(E_2^*, T)]. \quad (9)$$

This can be simplified by representing  $E_1^*$  and  $E_2^*$  as a ratio,  $E_r = E_2^*/E_1^*$ . The values of  $x$  and  $E_r$  depend only on the adsorbent solid and thus are completely independent of the gas molecule. In this work a single surface model is assumed, but nonporous and porous surfaces are represented by different arrangements of graphene sheets.

## Experimental

The experimental portion of this work was performed by Dr. Howard Thomas and students over a period of years. This work is part of an ongoing collaboration between Dr. Rybolt and Dr. Thomas in the study of surface phenomenon (15-19).

The adsorption data on the Carbopack C surface was collected by Dr. Thomas and Azuree B. Waters (15). Gas-solid second virial coefficient values were determined for a series of seventeen adsorbates using a Perkin-Elmer 3920A gas chromatograph with a thermal conductivity detector. Data were collected over a range of temperatures as close as possible to 403.5 K, with measurements being made at 403.5 +/- 0.5 K when possible. The primary molecular adsorbates were trichlorofluoromethane, butane, bromochloromethane, 1-chloro-2-methylpropane, dibromodifluoromethane, trichloromethane, dichlorodifluoromethane, chlorodifluoromethane, chloromethane, dichloromethane, propane, n-pentane, n-hexane, tetrachloromethane, 1,2-dichloropropane, 1-chlorobutane, and cyclohexane. The details of the experimental method used for each of the seventeen adsorbates can be found in the published paper (15). The gas chromatograph stainless-steel column was packed by Supelco Inc. with 2.78 g of the Carbopack C adsorbent, having BET N<sub>2</sub> adsorption surface area of 10 m<sup>2</sup>/g. Before measurements were performed, the column was outgassed for at least fourteen hours at a maximum temperature of 623 K to remove any residual sample from the surface. A Hamilton gas syringe was used to inject adsorbate samples, and a Hewlett-Packard 3392A integrator was used to record retention times and peak areas. Neon was used as the marker gas, a gas injected into

the column to determine the time required for a gas to pass through the column with no interactions with the surface. When determining the retention time for sample adsorbates, the retention time for the marker gas is subtracted from the actual retention time for the adsorbate (see Equation 1). The flow rates were measured with a soap bubble flow meter. Measurements of the retention time for each adsorbate were taken several times at each temperature, varying only the amount of gas injected. The retention times were calculated using Equation 1 and plotted versus injection volume. From this, it is possible to extrapolate to zero sample size, and then to use that value in the calculation of  $B_{2s}$ .

The adsorption data on the Carbosieve SIII surface were collected by Dr. Howard Thomas and a student during the summer of 2004. Gas-solid second virial coefficient values were determined for a series of nine adsorbate gases using a Perkin-Elmer 3920A gas chromatograph with a thermal conductivity detector. Data were collected within the temperatures limits of 342 K to 613 K with a range of about 30 degrees for each gas. The primary molecular adsorbates were methane, ethane, propane, butane, 2-methylpropane, chloromethane, chlorodifluoromethane, dichloromethane, and dichlorodifluoromethane. The gas chromatograph stainless-steel column was packed with Carbosieve SIII adsorbent by Supelco Inc., having BET  $N_2$  adsorption surface area of  $995 \text{ m}^2/\text{g}$ . Before measurements were performed, the column was outgassed to remove any residual sample from the surface prior to making adsorption measurements. The retention time measurements were identical to

those taken with Carbopack C, with the exception that these values were averaged and not extrapolated to zero coverage.

## **Analysis and Results**

### Building a Testable Surface

In order to test interactions between molecules and surfaces, an appropriate surface for testing had to be modeled. The modeling was done with CAChe software using augmented MM3 mechanics. MM3 was used because the structures were quite large with thousands of atoms, and more advanced methods of calculations could take days with such large structures. Graphite was chosen as the surface because the arrangement of carbon in aromatic, hexagonal rings connected in layers is very similar to the adsorbent carbon surface in the GC column.

Two problems when building the graphite surface were the need for the surface to be flat and to be uniform. First, the bond pattern CAChe applied for aromatic rings needed to be determined. While a mechanics calculation would show CAChe recognized all rings as aromatic, the placement of double bonds did not occur in any deducible pattern. In order to solve this problem, the layers were originally built starting from one benzene ring and subsequently increasing the size of the layer through addition of rings.

The second problem was that when the graphene layers were run in the mechanics program, it caused a bend or ripple to appear in the layer, as can be seen in Figure 2. After several different building methods were attempted to keep the layer symmetric, one flat, aromatic unit was built, the structure locked, and then the units were repeated and connected in order to create one large layer. The chosen repeat unit is shown in Figure 3. At this point the hydrogen on the outer rings of the layer

were eliminated from the structure. This was done because the molecules would be tested on the center of the large layer where rings would be aromatic. Also, it was assumed removing hydrogen would eliminate hydrogen repulsion around the edge of the molecule and possibly eliminate the ripple. This made the bend less pronounced but still present. The next approach was to copy a layer, rotate it so that the ripples were oppositely facing each other, as shown in Figure 4, and run mechanics. This method worked and produced the first flat, uniform graphene layer, which is shown in Figure 5.

#### Determining Necessary Ring Number

Graphene layers were built containing benzene ring numbers ranging from one to four hundred and thirty-two. Experiments were run using augmented MM3 parameters in CAChe with each layer and neon, argon, krypton, and xenon to determine  $\Delta E$  values in units of kcal/mol.  $\Delta E$  values were calculated by first running a mechanics calculation with the layer and the gas molecule far apart ( $E_{\text{apart}}$ ) and then running a mechanics calculation with the layer and the gas molecule touching ( $E_{\text{close}}$ ) and found the difference:  $\Delta E = |E_{\text{close}} - E_{\text{apart}}|$ .  $\Delta E$  is due to van der Waals force. The  $\Delta E$  values were then plotted versus the number of rings within each layer and the graphs examined to see where the points leveled off. As one can see in Figure 6, this leveling off occurs around 50-120 rings, so to be on the safe side the necessary number of rings was chosen to be one hundred and twenty-seven.

### Determining Necessary Layer Number

The graphene layer with 127 benzene rings was used to construct two, three, four, and five layered graphite structures. The structure composed of three layers is shown in Figure 7 with a xenon molecule. Similar experiments to those described above with neon, argon, krypton, and xenon and 1-5 layers were run using the same method of determining  $\Delta E$ . The  $\Delta E$  values were then plotted versus the number of layers within each structure and the graphs examined to see where the points leveled off. As can be seen in Figure 8, this leveling off occurs at three layers. The van der Waals range calculated in MM2 and MM3 is set at a default value of 9.0 Angstroms. This value was used in all modeling work.

### Determining Experimental $E^*$ values for Carbosieve SIII and Carbopack C

The Carbosieve SIII experimental data shown in Table 1 were initially analyzed by plotting the natural logarithm of  $B_{2s}$  versus the reciprocal of the temperature in Kelvin. As can be seen in Figure 9, this plot similarly produces a linear regression for all nine molecules tested on Carbosieve SIII. The slope of the linear regression produced is equal to the experimental  $E^*$  value, or gas-solid interaction energy.

The experimental data for Carbopack C was selected from a previously published paper (15). While seventeen adsorbates had determined  $B_{2s}$  values within this paper, only experimental data for ten adsorbates were used in this project. These

B<sub>2s</sub> data can be seen in Table 2, and were analyzed the same way that the Carbosieve SIII experimental data were analyzed.

### Testing Molecule-Surface Interactions and Comparing Experimental Values with Calculated Values for Carbosieve SIII

To test molecule-surface interactions with Carbosieve SIII, the nine molecules were constructed using CAChe and tested with a three layer graphite structure.  $\Delta E$  values were calculated for each molecule-surface interaction and converted to Ecal\* in units of Kelvin by multiplying by the constant, 503.2 K mol kcal<sup>-1</sup>. This conversion factor was determined by taking 1 kcal/mol and converting it to units of K mol kcal<sup>-1</sup> by using basic conversion, Avogadro's number, and the Boltzmann constant. The values of experimental E\* and calculated Ecal\* on the nonporous, or flat, surface can be found in Table 3. The nonporous model gave an r<sup>2</sup> value of 0.864, a slope equal to 1.9062, an average Ecal\*/E\* ratio of 0.550, and an average percent error equal to 45% for the experimental interaction energy values versus the calculated values. Because Carbosieve SIII is a nanoporous carbon, the values for Ecal\* on a flat surface were all low compared to experimental values.

To better model Carbosieve SIII within CAChe, a pore was created using two parallel sets of the structures containing three layers with each layer consisting of 127 rings. The pore size, d= 0.55 nm, was based on a pore adsorption analysis for Carbosieve SIII. The pore diameter d is the separation between the outer edge of carbon atoms lining the pore, while D is the separation of carbon nuclei on the two

layers adjacent to the pore opening. In graphite carbon layers are 0.34 nm apart, and the carbon atom radius is 0.17 nm. Therefore the pore internuclei separation,  $D$ , is related to the pore diameter,  $d$ , by  $D = d + 0.34$ .

The nine molecules were individually placed into this pore, at an equal distance from the two nearest interior walls, to find  $E_{cal}^*$  values for the interaction energy. The  $E_{cal}^*$  values for each molecule with the nanoporous surface model are given in Table 4. The plot of  $E^*$  versus  $E_{cal}^*$  for the nanoporous model gave an  $r^2$  value of 0.962, a slope equal to 1.6129, an average  $E_{cal}^*/E^*$  ratio of 0.618, an average percent error equal to 38%, and is shown in Figure 10. Also, an example of hexane between the two sets of layers is shown in Figure 11.

The nine molecules were then tested in pores of varied sizes to test if another pore size, other than 0.55 nm, gives a better  $r^2$  value in relation to experimental  $E^*$  values. Each of the nine molecules was tested in each pore size and plots of  $E^*$  versus  $E_{cal}^*$  were produced. The  $r^2$  values from each of the different pore sizes were then plotted against the diameters of the pores, and the plots were examined to see which diameter gave the highest  $r^2$  value. This plot is shown in Figure 12, and it can be seen that 0.50 nm gave the best  $r^2$  value of 0.980. This plot had a slope of 1.345, in relation to experimental  $E^*$  values. These values of slope,  $r^2$ , average  $E_{cal}^*/E^*$ , and average percent error can be found in Table 5 for both nonporous, or flat, and nanoporous surface models for Carbosieve SIII.

### Testing Molecule-Surface Interactions and Comparing Experimental Values with Calculated Values for Carbopack C

To test molecule-surface interactions with Carbopack C, the seventeen experimentally used molecules were constructed using CAChe and tested with one three layer graphite structure.  $\Delta E$  values were calculated for each molecule-surface interaction and converted to  $E_{cal}^*$  by multiplying by the constant,  $503.2 \text{ K mol kcal}^{-1}$ . The  $E_{cal}^*$  values for each molecule with one set of three layers, nonporous or flat surface model, are given in Table 6. The plot of  $E^*$  versus  $E_{cal}^*$  for the nonporous model gave an  $r^2$  value of 0.927, a slope equal to 1.1153, an average  $E_{cal}^*/E^*$  ratio of 1.303, an average percent error equal to 10%, and is shown in Figure 13.

The seventeen molecules were also tested in a 0.55 nm pore to test if CAChe better represents the flat or porous surface model for Carbopack C. The seventeen molecules were individually placed into this pore to get  $E_{cal}^*$  values for the interaction energy. The nanoporous model gave an  $r^2$  value of 0.945, a slope equal to 0.7609, an average  $E_{cal}^*/E^*$  ratio of 1.303, and an average percent error equal to 30% for the experimental interaction energy values versus the calculated values for Carbopack C. These values of slope,  $r^2$ , average  $E_{cal}^*/E^*$ , and average percent error can be found in Table 7 for both nonporous, or flat, and nanoporous surface models for Carbopack C.

## Discussion

An important result of this study is the conclusion that one can use CAChe to accurately represent carbon surfaces, both nonporous and nanoporous. This was confirmed for the Carbosieve SIII surface through the improvement made in the gas-surface interaction energies when changing from a nonporous or flat model to a nanoporous model. The same is true for the Carbopack C surface when changing from the nanoporous model to the nonporous or flat model.

A summary of the differences between the nonporous and nanoporous model results for Carbosieve SIII can be found in Table 5. The porous model gives better results for the values of  $r^2$ , average  $E_{cal^*}/E^*$ , and average percent error. This supports the fact that CAChe can accurately represent the nanoporous surface of Carbosieve SIII to give reliable gas-solid interaction energies.

The same can be seen by looking at the summary of differences between the nonporous and nanoporous model results for Carbopack C found in Table 7. The flat model gives better results for slope, average  $E_{cal^*}/E^*$ , and average percent error. This supports the fact that CAChe can accurately represent the nonporous or flat surface of Carbopack C to give reliable gas-solid interaction energies.

In addition to these results, the parameters of MM2 and MM3 were compared to determine if one gave better results than the other. For the linear regression results of  $E^*$  values for the nonporous, flat model MM2 gave a  $r^2$  value of 0.90 while MM3 gave a  $r^2$  value of 0.78. Going from a flat surface model to a nanoporous surface model gave a  $r^2$  value of 0.96 for MM2 and a  $r^2$  value of 0.91 for MM3. Clearly the

MM2 parameters give better results than MM3, and the experimental  $E^*$  values are best correlated by the MM2 nanoporous model.

As shown in Figure 12, 0.50 nm gave the best  $r^2$  value of 0.980, with a slope of 1.345, in relation to experimental  $E^*$  values. The optimal pore size can be determined because of the variation in potential energy curves for each molecule in the set. If the pore was too small, larger molecules were not able to fit, and repulsion experienced by the molecules was high due to narrow pore walls, thus greatly decreasing the  $r^2$  value. If the pore was too large, the interaction was decreased and thus the  $r^2$  value decreased, but not as dramatically as when the pore size was too small.

It is apparent by comparison of several factors,  $r^2$  values, slopes,  $E_{cal^*}/E^*$  ratios, and percent errors, that CAChe software can accurately correlate the physical properties of a molecule. Basically, CAChe was used to build representative models of both Carbosieve SIII and Carbopack C. These models were shown to give gas-solid interaction energies that reflected experimentally obtained interaction energies from gas chromatography. This has important implications because if  $E^*$  values can be accurately predicted using CAChe or other computational techniques then they in turn can be used to predict  $B_{2s}$  values. These values can be used to relate the structure of molecules and the nature of carbon surfaces to experimentally measured properties. From these calculations, Quantitative Structure Retention Relations (QSRR), which represent statistical models that quantify the connection between the molecular structure and the chromatographic retention times, can be developed to correlate the

experimental and computed properties. These QSRR values might be used to predict the separation of gas mixtures or the amounts of gas adsorbed onto carbon surfaces. These values could have important applications in fields such as chemical warfare protection, environmental clean-up, and carbon filters for air purification.

## Conclusion

The significance of this work is that it demonstrates how CAChe calculations can be used to accurately represent carbon surface structures. This representation has been shown using flat, Carbopack C, and porous, Carbosieve SIII, structures. It should be noted that it was through comparison of a combination of factors ( $r^2$ , slope,  $E_{cal^*}/E^*$ , and percent error) that determinations of which structure better represented experimental values were made as opposed to using an individual factor as a predictor alone.

Some possible future work would be to look at other carbon surface structures and determine if CAChe can be used to accurately predict gas-solid interaction energies for them as well. The future applications of these molecule-carbon interactions could include: removing odor molecules, storing gases for energy production, detecting molecules through electronic nose devices, predicting gas chromatography retention times, separating molecular mixtures, protecting from chemical warfare agents, monitoring the environment, and removing organic pollutants.

## References

1. J.O. Hirschfelder, C.F. Curtiss, R.B. Bird, *Molecular Theory of Gases and Liquids*, John Wiley & Sons, Inc., New York, 1954.
2. K.E. Drexler, *Nanosystems: Molecular Machinery, Manufacturing, and Computation*, Wiley-Interscience, New York, 1992, pp. 1-70.
3. Y. Shuxia, C. Wang, B. Xu, C. Bai, *J. Phys. Chem. B* 106 (2002) 9044.
4. D.C. Sorescu, K.D. Jordan, *J. Phys. Chem. B* 105 (2001) 11227.
5. A. Montoya, T.N. Truong, A.F. Sarofim, *J. Phys. Chem. A* 104 (2000) 6108.
6. K. Murata, K. Kaneko, W.A. Steele, F. Kokai, K. Takahashi, D. Kasuya, M. Yudasaka, S. Iijima, *Nano Letters* 1 (2001) 197.
7. A.R. Katritzky, M. Karelson, V.S. Lobanov, *Pure & Applied Chemistry* 69 (1997) 245.
8. I. Abe, H. Kamaya, I. Ueda, *Journal of Pharmaceutical Science* 77 (1988).
9. H. Jankowska, A. Swiatkowski, J. Choma, *Active Carbon*, Ellis Horwood, New York, 1991, pp. 75-100.
10. C.H. Reynolds, *Journal of Molecular Structure* 401 (1997) 267.
11. M. Comet, L. Schreyeck, S. Verdan, G. Burato, H. Fuzellier, *Journal of Chemical Education* 81 (2004) 819.
12. C. Dapeng, P. Feng, J. Wu, *Nano Letters* 4 (2004) 1489.
13. N. Shukla, J. Gui, A.J. Gellman, *Langmuir* 17 (2001) 2395.
14. S. Kwon, J. Russell, X. Zhao, R.D. Vidic, J.K. Johnson, E. Borguet, *Langmuir*, 18 (2002) 2595.
15. T.R. Rybolt, D.L. Logan, M.W. Milburn, H.E. Thomas, A.B. Waters, *Journal of Colloid Interface Science* 220 (1999) 148-156.
16. T.R. Rybolt, H.E. Thomas, *Interfacial Phenomena in Chromatography*, Ed. Emile Pefferkorn, Marcel-Dekker, New York, 1999, pp. 1-40.

17. T.R. Rybolt, V.E. Janeksela, D.N. Hooper, H.E. Thomas, N.A. Carrington, E.J. Williamson, *Journal of Colloid Interface Science* 272 (2004) 35.
18. T.R. Rybolt, D.N. Hooper, J.B. Stensby, H.E. Thomas, M.L. Baker, *Journal of Colloid Interface Science* 234 (2001) 168.
19. T.R. Rybolt, R.A. Pierotti, *Journal of Chemical Physics* 70 (1979) 4413.

**Table 1**  
 Second gas-solid virial coefficients from gas-solid chromatography  
 Carbosieve SIII

Adsorbate	T (K)	$B_{2s}$ (cm <sup>3</sup> /g)
Methane	342.8	29.1
	352.5	23.7
	362.4	19.7
	372.3	16.3
Ethane	426.7	92
	436.6	74.6
	446.5	60.1
	456.4	49.0
Propane	520.9	89
	530.7	72
	541.1	59
	551.5	48
Isobutane	541.1	54
	551.1	42
	561.7	32
	571.7	24.8
n-Butane	571.9	162
	582.5	138
	592.3	109
	602.5	90
	612.5	69
Chloromethane	460.5	113
	470.3	93
	480.3	76
	490.2	63
Dichlorodifluoromethane	480.5	50
	490.1	38
	500.2	28
	510.2	21

Chlorodifluoromethane	500.6	41
	510.2	34
	520.3	27
	530.4	22
Dichloromethane	581.1	93
	591.1	78
	601.5	67
	611.5	56

**Table 2**  
 Second gas-solid virial coefficients from gas-solid chromatography  
 Carbopack C

Adsorbate	T (K)	$B_{2s}$ (cm <sup>3</sup> /g)
Dichlorodifluoromethane	363.2	0.902
	332.8	2.34
	343.4	1.69
	353.6	1.12
	323.2	2.93
	343.6	1.67
Propane	363.2	0.688
	323	2.25
	332.8	1.66
	343.4	1.16
	353.6	0.817
Chlorodifluoromethane	332.8	0.582
	313.6	0.89
	323.2	0.681
	308.9	1.2
	343.6	0.442
Chloromethane	313.4	0.779
	323.2	0.583
	308.9	1.00
	333.8	0.507
	313.3	0.873
1,2-Dichloropropane	452.7	2.78
	473	1.57
	492.9	1.03
	483.6	1.27
	493.3	1.02
	433.3	4.75
	443.1	3.5

1-Chlorobutane	452.7	2.74
	473	1.54
	492.9	0.994
	483.6	1.23
	433.3	4.4
	493.1	1.05
	443.1	3.48
	453.1	3.25
	443.5	2.51
	433.3	4.79
	472.4	1.61
483.1	1.24	
n-Pentane	452.7	1.7
	432.3	2.73
	423.5	3.81
	442.5	2.02
	433.3	2.59
Dichloromethane	392.9	0.848
	372.9	1.4
	363.2	1.87
	343.7	3.93
	353.5	2.41
	343.6	3.91
	382.8	1.19
n-Hexane	452.7	7.47
	463.2	4.92
	472.6	3.45
	482.9	2.88
	493.6	2.1
Trichloromethane	452.7	0.86
	432.3	1.23
	412.9	2.18
	423.5	1.65
	403.4	2.67
	433.3	1.22

**Table 3**  
Calculated gas-solid interaction energies (K) with MM2  
Carbosieve SIII – Flat Surface Model

Formula	Name	Expt E*	Flat Ecal*
CH <sub>4</sub>	Methane	2495	1739
C <sub>2</sub> H <sub>6</sub>	Ethane	4142	2349
C <sub>3</sub> H <sub>8</sub>	Propane	5766	3346
C <sub>4</sub> H <sub>10</sub>	n-Butane	8080	4147
CH <sub>3</sub> CH(CH <sub>3</sub> ) <sub>2</sub>	Isobutane	7872	3465
CH <sub>3</sub> Cl	Chloromethane	4452	2586
CHClF <sub>2</sub>	Chlorodifluoromethane	5599	2853
CH <sub>2</sub> Cl <sub>2</sub>	Dichloromethane	5851	3369
CCl <sub>2</sub> F <sub>2</sub>	Dichlorodifluoromethane	7186	3492

**Table 4**  
Calculated gas-solid interaction energies (K) with MM2  
Carbosieve SIII –Porous Surface Model

Formula	Name	Expt E*	Nanoporous Ecal*
CH <sub>4</sub>	Methane	2495	1519
C <sub>2</sub> H <sub>6</sub>	Ethane	4142	2623
C <sub>3</sub> H <sub>8</sub>	Propane	5766	3667
C <sub>4</sub> H <sub>10</sub>	n-Butane	8080	4739
CH <sub>3</sub> CH(CH <sub>3</sub> ) <sub>2</sub>	Isobutane	7872	4870
CH <sub>3</sub> Cl	Chloromethane	4452	2651
CHClF <sub>2</sub>	Chlorodifluoromethane	5599	3120
CH <sub>2</sub> Cl <sub>2</sub>	Dichloromethane	5851	3999
CCl <sub>2</sub> F <sub>2</sub>	Dichlorodifluoromethane	7186	4628

**Table 5**  
Carbosieve SIII – Porous (d=0.55 nm)  
Linear Regression Results Using MM2 Parameters  
 $E^* = a E_{cal}^*$

Model	Slope	r <sup>2</sup>	Avg $E_{cal}^*/E^*$	Avg % Error
Flat	1.9062	0.864	0.550	45.00
<b>Porous</b>	<b>1.6129</b>	<b>0.9624</b>	<b>0.618</b>	<b>38.18</b>

**Table 6**  
 Calculated gas-solid interaction energies (K) with MM2  
 Carbopack C – Flat Surface Model

Formula	Name	Expt E*	Flat Ecal*
CHCl <sub>3</sub>	Trichloromethane	4601	3917
CCl <sub>2</sub> F <sub>2</sub>	Dichlorodifluoromethane	3957	3388
CHClF <sub>2</sub>	Chlorodifluoromethane	3172	2767
CH <sub>3</sub> Cl	Chloromethane	2488	2496
CH <sub>2</sub> Cl <sub>2</sub>	Dichloromethane	3563	3252
C <sub>3</sub> H <sub>8</sub>	Propane	2866	3252
C <sub>5</sub> H <sub>12</sub>	n-Pentane	4501	5071
C <sub>6</sub> H <sub>14</sub>	n-Hexane	5293	5958
C <sub>3</sub> H <sub>6</sub> Cl <sub>2</sub>	1,2-Dichloropropane	4323	4283
(CH <sub>3</sub> ) <sub>3</sub> CCl	1-Chlorobutane	4731	5062

**Table 7**  
Carbopack C – Flat (d=0.55 nm for Porous)  
Linear Regression Results Using MM2 Parameters  
E\* = a Ecal\*

Model	Slope	r2	Avg Ecal*/E*	Avg % Error
<b>Flat</b>	<b>1.1153</b>	0.9270	<b>0.899</b>	<b>10.10</b>
Porous	0.7609	<b>0.9448</b>	1.303	30.27

**Figure 1**  
The Lennard-Jones potential energy well.

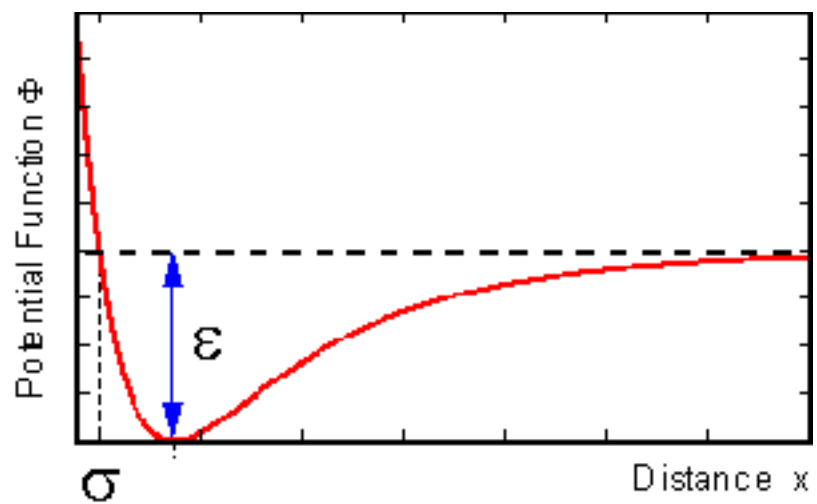


**Figure 2**

The bend or ripple which appeared in the graphene layer following mechanics calculations.



**Figure 3**  
The chosen repeat unit to build a graphene layer.

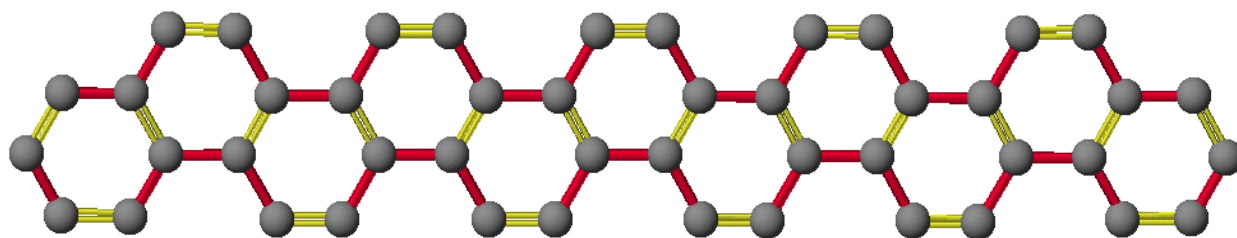


**Figure 4**

To correct the ripple, a layer was copied and rotated so that the ripples oppositely faced each other and then the two layers were run in mechanics.

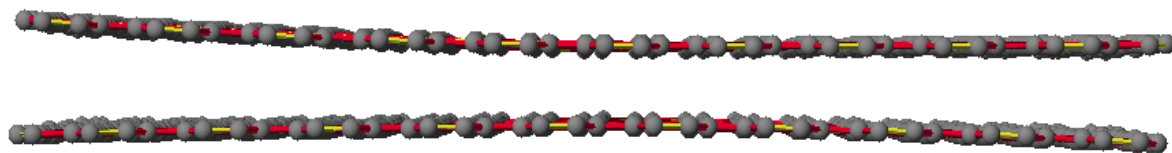


**Figure 5**

The first flat, uniform graphene layer was created. This layer is shown in ball-and-stick, line, and space filling models.

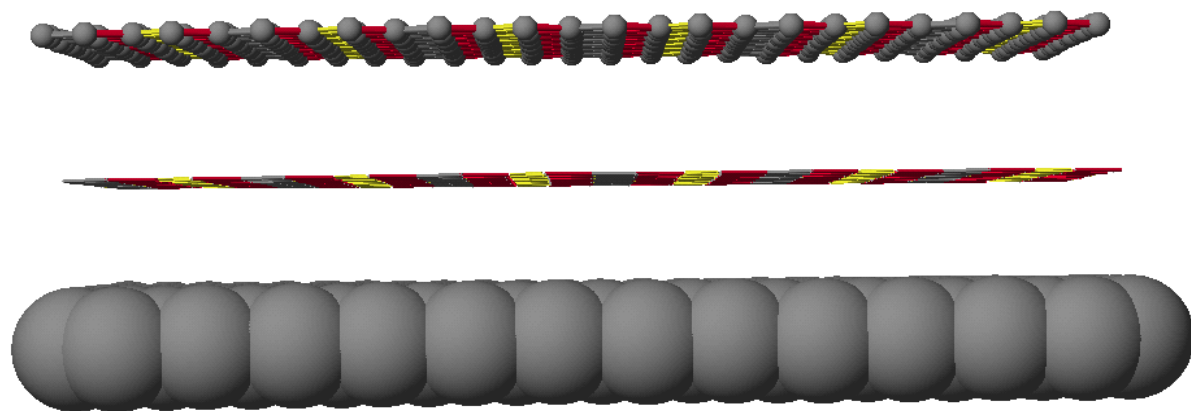


**Figure 6**

The plot of  $\Delta E$  for each of the gases (Ne, Ar, Kr, Xe) versus the number of rings within each layer to determine the necessary number of rings.

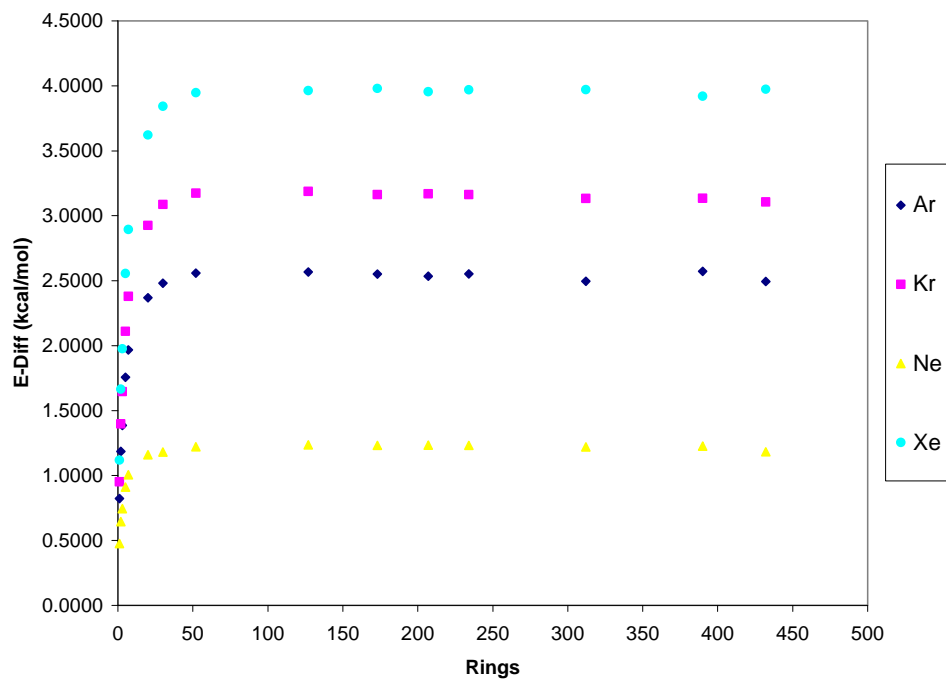


**Figure 7**

A xenon molecules being tested with a three layer graphite structure.

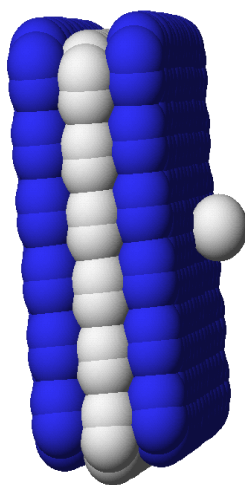


**Figure 8**

The graph of  $\Delta E$  versus the number of layers within each structure to determine the necessary number of layers.

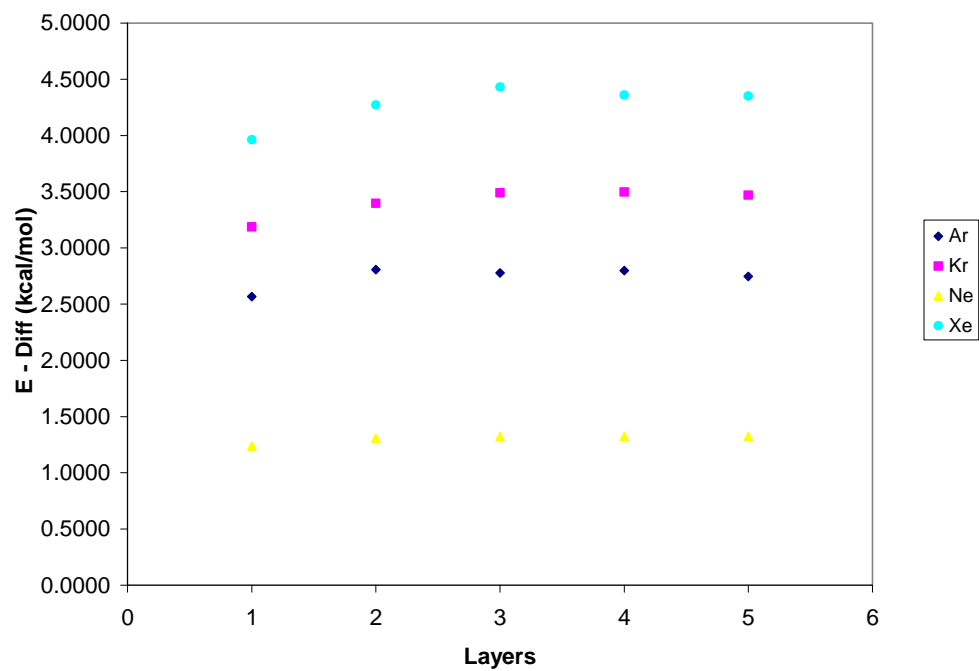


**Figure 9**  
A plot of  $\ln B_{2s}$  versus  $1/T$  (K) for Carbosieve SIII.

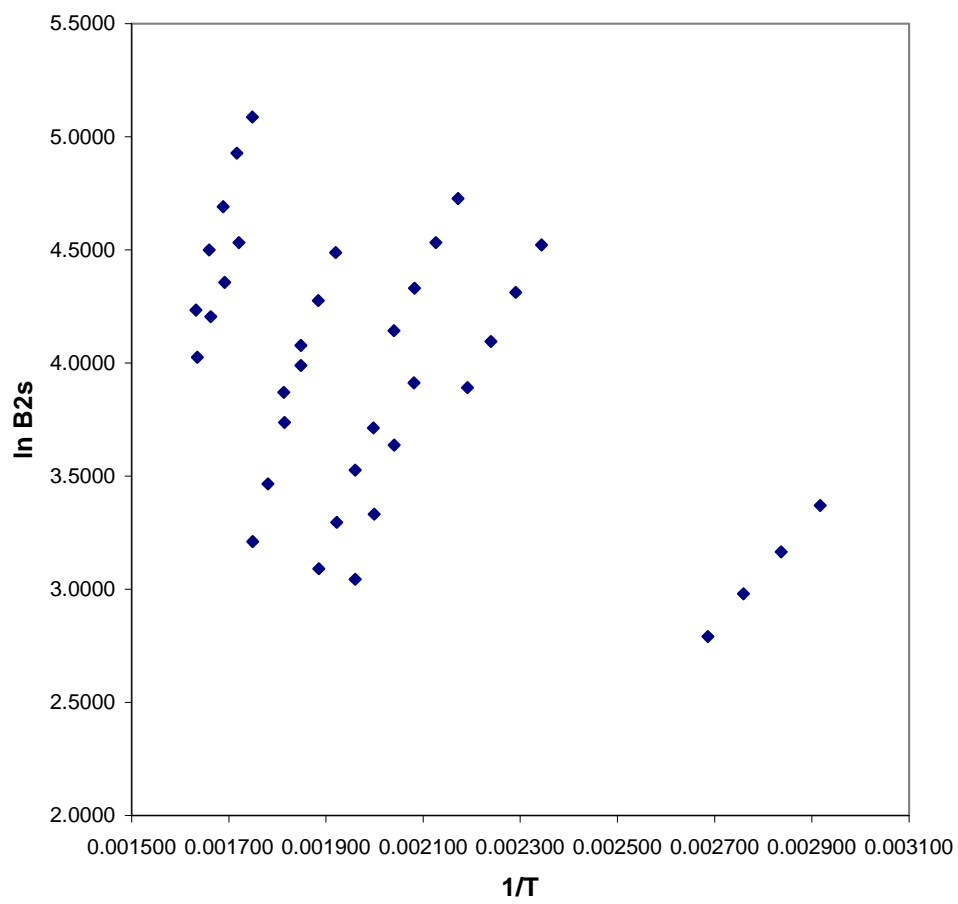


**Figure 10**

A plot of  $E^*$  versus  $E_{cal}^*$  for the nanoporous model for Carbosieve SIII for  $d=0.55$  nm.

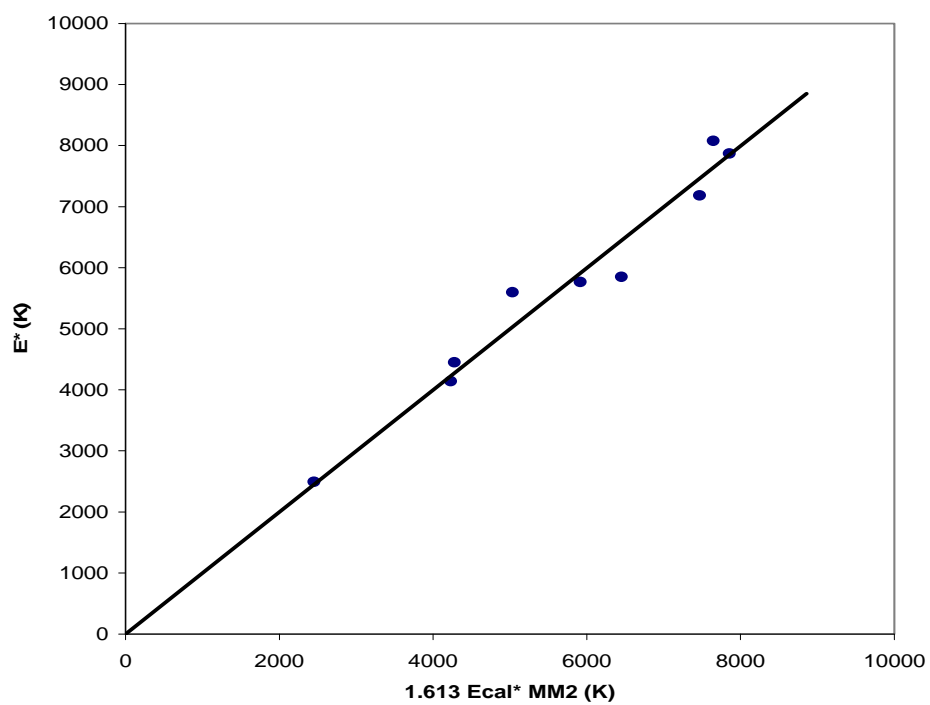


**Figure 11**  
Hexane in a 0.55 nm pore.

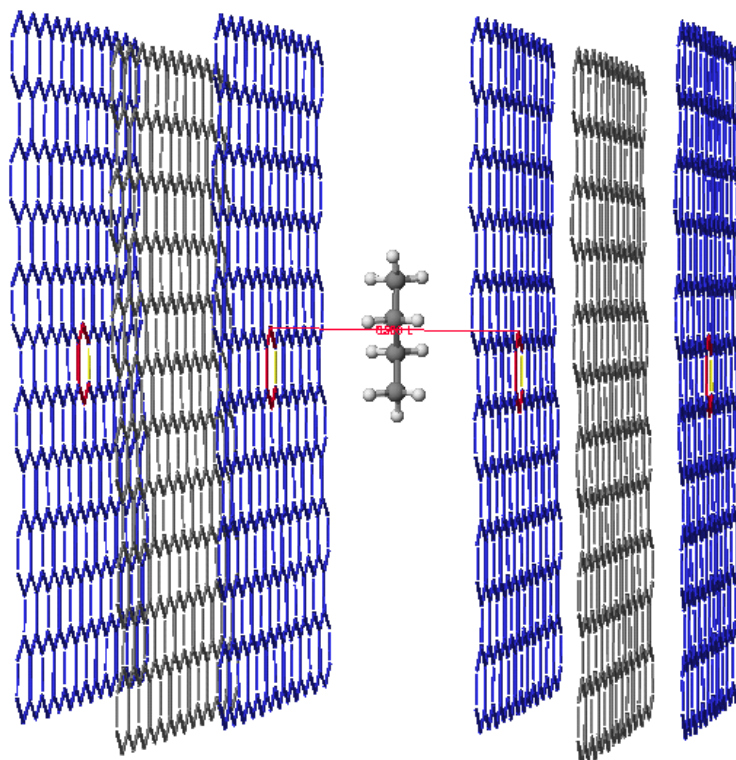


**Figure 12**  
A plot of  $r^2$  versus diameter for varied pore sizes.

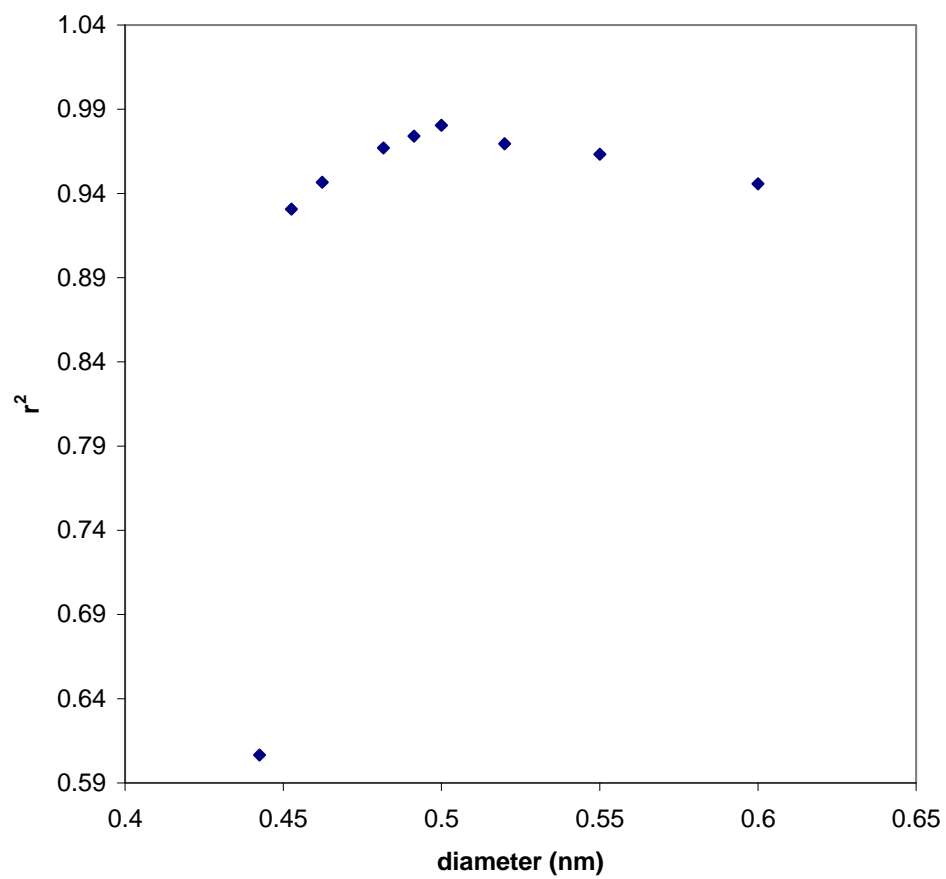


**Figure 13**

A plot of  $E^*$  versus  $E_{\text{calc}}^*$  for the flat model for Carbopack C.

